THE JOURNAL OF GENE MEDICINE
J Gene Med 2009; **11**: 598–604.
Published online 27 April 2009 in Wiley InterScience (www.interscience.wiley.com) **DOI:** 10.1002/jgm.1337

RESEARCH ARTICLE

Enhanced transgene expression in the mouse skeletal muscle infected by the adeno-associated viral vector with the human elongation factor 1α promoter and a human chromatin insulator

Mayuyo Mori-Uchino[1,2†]
Takamasa Takeuchi[1†]
Isao Murakami[1,3]
Tetsu Yano[2]
Toshiharu Yasugi[2]
Yuji Taketani[2]
Keiichi Nakagawa[4]
Tadahito Kanda[1*]

[1]*Center for Pathogen Genomics, National Institute of Infectious Diseases, Tokyo, Japan*

[2]*Department of Obstetrics and Gynecology, Faculty of Medicine, The University of Tokyo, Tokyo, Japan*

[3]*Department of Obstetrics and Gynecology, School of Medicine, Keio University, Tokyo, Japan*

[4]*Department of Radiology, Graduate School of Medicine, The University of Tokyo, Tokyo, Japan*

*Correspondence to:
Tadahito Kanda, Center for Pathogen Genomics, National Institute of Infectious Diseases, 1-23-1 Toyama, Shinjuku-ku, Tokyo 162-8640, Japan.
E-mail: kanda@nih.go.jp

†Both investigators contributed equally and should be considered as senior authors.

Received: 11 September 2008
Revised: 26 January 2009
Accepted: 18 March 2009

Abstract

Background Efficient and continuous expression of a therapeutic transgene is a key factor for improving the efficacy of gene therapy. Some insulators are known to contribute to continuous high-level expression of a therapeutic transgene.

Methods Using the human AAVS1 insulator (DHS) found in the AAVS1 DNase I hypersensitive site, chicken β-globin insulator (cHS4) and sea urchin arylsufatase insulator (Ars), we newly constructed three recombinant adeno-associated virus vectors (rAAV) and examined their capability of transducing the mouse quadriceps muscle.

Results DHS increased transgene expression from the human elongation factor 1α promoter (EF) by 1000-fold, up to the high level achieved by the human cytomegalovirus immediate early promoter/enhancer (CMV), which comprises an extremely strong promoter for driving a transgene. cHS4 enhanced the expression by 100-fold, whereas Ars did not. The enhanced expression was maintained for at least 24 weeks. Vector copy numbers were similar with and without DHS or cHS4; thus, the enhancement is most likely due to up-regulated transcription. Neither DHS, nor cHS4 affected transgene expression from CMV. DHS enhanced expression from the human muscle creatine kinase promoter/enhancer by 100-fold in mice, as did DHS from EF.

Conclusions Although DHS was unable to further enhance high expression from the strong viral enhancer/promoter, it enhanced low expression from the human promoters by 100- to 1000-fold. Thus, DHS may be useful for constructing rAAVs that express a therapeutic transgene from less efficient, tissue specific promoters. Copyright © 2009 John Wiley & Sons, Ltd.

Keywords AAV vector; insulator; transduction of muscle

Introduction

Recombinant adeno-associated virus vector (rAAV), which is highly stable and can infect various organs, is considered to be suitable for *in vivo* administration in gene therapy [1,2]. Because the rAAV genome lacks the viral rep gene, whose product mediates the viral DNA replication and the integration of the viral DNA into the AAVS1 region in chromosome 19, the rAAV genome is

not replicable and does not undergo site-specific integration [3,4]. Recent studies have shown that the vast majority of infected rAAV genomes persist in the muscle in an extra-chromosomal circular form [5–7]. A variety of integration junctions between the rAAV genome and host chromosome have been recovered, indicating that a small fraction of the infected rAAV genomes is integrated at random sites [8]. The expression of transgene introduced by rAAV lasts for a long time, and some successful animal data have allowed human clinical trials to be conducted using rAAVs for the treatment of cystic fibrosis, hemophilia B, and Parkinson's disease [9–11].

Efficient and continuous expression of a therapeutic transgene is a key factor for improving the efficacy of gene therapy. Insulators comprise an element with the potential to induce continuous high-level expression of a transgene. Insulators have been shown experimentally to comprise the DNA sequences that define a domain of gene expression by directionally protecting a promoter from enhancers in different domains and by acting as a boundary to the surrounding heterochromatin [12]. Heterochromatinization is associated with silencing epigenetic modifications, including histone deacetylation and DNA methylation. Insulators appear to have mechanisms that counteract the silencing effects of heterochromatin [13,14].

In previous studies, insulators were inserted into vector genomes to protect their transgene expression cassettes from the negative influences brought about by adjacent elements. Expression of the transgene integrated in the host chromosome with a lentivirus vector carrying the chicken β-globin insulator is two-fold higher than that with the insulator-less vector [15]. The chicken β-globin insulator inserted into an adenovirus vector shields a downstream promoter from viral enhancers or silencers that are present in the vector genome [15–18].

In the present study, we constructed rAAVs with the selected insulator and injected them into the skeletal muscle of mice. Because previous studies have indicated that the great majority of rAAV genomes are maintained as extra-chromosomal concatemers, the muscle is an appropriate organ to target when aiming to avoid dilution of vector genomes by host cell division. The insertion of the insulator enhanced transgene expression from the human elongation factor 1α promoter and human muscle creatine kinase promoter/enhancer but did not affect expression from the human cytomegalovirus immediate early promoter/enhancer. These data suggest that the insulator has capacity to enhance transgene expression from a less efficient promoter.

Materials and methods

Vector plasmids

The DNA fragment encoding luciferase, which was excised from pGL4.10 (Promega Corp., Madison, WI, USA) by digestion with *Kpn*I and *Xba*I, was inserted between *Kpn*I and *Xba*I in the multiple cloning site of pEF1/Myc-HisA (Invitrogen Corp., Carlsbad, CA, USA) to yield pEF1α-luc containing a luciferase expression cassette driven by the human elongation factor 1α promoter (EF). pAAV-hrGFP (Stratagene, La Jolla, CA, USA) was digested with *Xho*I and treated by a DNA Blunting Kit (Takara-Bio Inc., Otsu, Japan), followed by further digestion with *Mlu*I, and then electrophoresed on an agarose gel. The DNA fragment containing plasmid backbone, two inverted terminal repeats (ITRs), and hGH-polyA signal (pAAV-ITR) was extracted from the gel. The luciferase expression cassette, which was excised by digestion of pEF1a-luc with *Mlu*I and *Pme*I, was ligated with pAAV-ITR to generate pAAV-EF1-Luc. pAAV-EF1-Luc was digested with *Mlu*I and treated by DNA Blunting Kit, followed by the insertion of *Bam*HI linker to add a *Bam*HI site for the insertion of the insulator fragment. The DHS-S1 region (352 bp, nucleotides 27897527–27897176 of NT_011109.15) [19] was amplified from HeLa genomic DNA by polymerase chain reaction (PCR) with a forward primer having a *Bam*HI site and a reverse primer having a *Bgl*II site, and the resultant fragment was designated as DHS. The chicken β-globin insulator core region (244 bp) [20] and the sea urchin arylsufatase insulator region (578 bp) [21] were generated by annealing of the synthetic complementary oligonucleotides with the sequences of these regions and the recognition sequences of *Bam*HI and *Bgl*II at the 5′ and 3′ ends and the resultant DNA fragments were designated as cHS4 and Ars, respectively. Stuffer, a transcriptionally inert DNA fragment, was amplified from a modified *Renilla* luciferase gene (nucleotides 1329–1679 of phRG-TK (Promega Corp.)) by PCR with a forward primer with a *Bam*HI site and a reverse primer with a *Bgl*II site. Stuffer and the insulator elements were inserted into the *Bam*HI site of pAAV-EF1-Luc to produce pAAV-EF-Stuffer, pAAV-EF-DHS, pAAV-EF-cHS4, and pAAV-EF-Ars, respectively.

A DNA fragment containing the human cytomegalovirus immediate early promoter/enhancer (CMV) and β-globin intron of pAAV-hrGFP was amplified by PCR using primers having *Hin*dIII sites at their 5′ ends. pAAV-EF-Stuffer, pAAV-EF-DHS, pAAV-EF-cHS4, and pAAV-EF-Ars were digested with *Hin*dIII to remove the promoter region (EF) and then ligated with the CMV fragment to produce pAAV-CMV-Stuffer, pAAV-CMV-DHS, pAAV-CMV-cHS4, and pAAV-CMV-Ars, respectively. The C2 site of CMV [22] was removed from pAAV-CMV-Stuffer and pAAV-CMV-DHS to produce pAAV-CMV/E(−)-Stuffer and pAAV-CMV/E(−)-DHS, respectively.

Human muscle creatine kinase enhancer and promoter regions were amplified from human keratinocyte genomic DNA by PCR with the primers for the enhancer (5′-GGATCCTCGAGCCACCCAGGGCCCCGT-3′ and 5′-CTCGAGGGAGGGTCTCGGTCGCCG-3′) and for the promoter (5′-CTCGAGGCCCAGGAAGGGCTGGTGGCTGAA-3′ and 5′-AAGCTTGGCTGGGCTGGGCTGAAGGGG-3′). After cloning the PCR-fragments into pGEM-T easy (Promega Corp.), the enhancer fragment was obtained

DOI: 10.1002/jgm

by digestion with *Bam*HI and *Xho*I and the promoter fragment was obtained by digestion with *Xho*I and *Hin*dIII. These two fragments were ligated at *Xho*I site to produce the human muscle creatine kinase promoter/enhancer (CKM) and then ligated with the larger fragment obtained by digestion of pAAV-EF1-Luc with *Bam*HI and *Hin*dIII. Stuffer and the insulator elements were inserted into the *Bam*HI site of the resulting plasmid to produce pAAV-CKM-Stuffer, pAAV-CKM-DHS, pAAV-CKM-cHS4, and pAAV-CKM-Ars, respectively.

Cells

The 293 FT cells were grown in the Dulbecco's modified Eagle's medium (Invitrogen Corp.) containing 10% fetal bovine serum, penicillin (50 μg/ml), kanamycin (100 units/ml) (growth medium) supplemented with G418 (500 μg/ml).

The C2C12 cells [23] were grown in the growth medium and passaged every other day.

rAAVs

The 293 FT cells (5×10^6) were seeded in a 10-cm poly D-lysine dish (BD Biosciences, San Jose, CA, USA) and incubated for 24 h. The cells were transfected with a mixture of a vector plasmid (3 μg) and a helper/packaging plasmid (pEEV-XX2) [24] (9 μg) by using 36 μl of Lipofectamine 2000 (Invitrogen Corp.) per dish. The medium was changed every 24 h with the growth medium supplemented with 1× non-essential amino acid (Invitrogen Corp.) twice. The cells were lysed by freeze–thaw 3 days after the transfection and rAAV was purified by the heparin affinity column method, as described previously [25].

The purified rAAV stock was treated with benzonase for 30 min at 37 °C, followed by overnight treatment of sodium dodecyl sulfate and proteinase K. Vector genome was then extracted by phenol/chloroform extraction, chloroform extraction, and ethanol precipitation. The rAAV genome copy number was measured by real-time PCR (7900HT Fast Real-Time PCR System; Applied Biosystems, Foster City, CA, USA) using Power SYBRGreen PCR Master Mix (Applied Biosystems). The PCR primers for the real-time PCR were set in the luciferase coding sequence. The forward primer was 5′-TTGTGTCCGATTCAGTCATGC-3′ (300 nM final concentration) and the reverse primer was 5′-GGTGAACATGCCGAAGCC-3′ (300 nM final concentration).

Assay of luciferase activity of C2C12 cells infected with the rAAV

The C2C12 cells (1×10^4) were seeded in a 96-well plate, incubated for 24 h, and then inoculated with the rAAV (1×10^8 genome copies). The cells were harvested at 72 h after inoculation and lysed with Passive Lysis Buffer (Promega Corp.). Luciferase activity was measured with Mithras LB940 (Berthold Technologies, Bad Wildbad, Germany) using Luciferase Assay Systems (Promega Corp.). The level of luciferase activity was exhibited in relative light units (RLU).

Assay of luciferase activity of mouse muscles injected with the rAAV

Female BALB/c mice (aged 4 weeks) purchased from Nippon SLC (Shizuoka, Japan) were used in accordance with the local institutional guidelines. The animal was anesthetized with diethyl ether and the quadriceps muscle was injected with rAAV suspended in phosphate-buffered saline (PBS) (50 μl). For comparison, some mice received plain PBS in a similar manner. The entire quadriceps muscle was removed, cut into small pieces (approximately 200 mg), and rapidly frozen on dry ice prior to luciferase analysis. The frozen muscle was mixed with passive lysis buffer with the ratio of 300 μl to 100 mg of tissue. The mixture was then homogenized with a Zirconium bead with MM300 (Retsch GmbH, Haan, Germany) at a frequency of 25 Hz for 15 min, and was left at room temperature for 15 min. The total homogenate of each leg was centrifuged at 12 000 r.p.m. (11 000 × g) for 5 min. The supernatant (20 μl) was used for the luciferase activity assay.

Assay of the vector genome copy number in the muscle

The mouse quadriceps muscle was injected with rAAV of 1×10^{10} genome copies. The muscle was isolated at 4 weeks after injection. Total DNA was extracted from the muscle by using Blood & Cell Culture DNA Midi Kit (Qiagen, Valencia, CA, USA) according to the manufacturer's instructions. The amount of the vector genome DNA in the sample was determined by TaqMan PCR. The TaqMan PCR primers and probe were set in the luciferase coding sequence. The forward primer was 5′-TTGTGTCCGATTCAGTCATGC-3′ (300 nM final concentration) and the reverse primer was 5′-GGTGAACATGCCGAAGCC-3′ (300 nM final concentration), and the probe was 5′-FAM-CTTCGGCAACCAGATCATCCCCG-TAMRA-3′ (200 nM final concentration). The TaqMan PCR conditions used were: 95 °C for 10 min, followed by 40 cycles of 95 °C for 15 s and 60 °C for 1 min in a 25-μl reaction volume. The level of vector DNA in the sample (25 ng of total muscle DNA) was estimated by comparison with the standard curve that had been produced using 1×10^1 to 1×10^5 copies of vector plasmid (coefficient of linearity ≥ 0.995). The result obtained was expressed as the rAAV DNA copy number per nucleus, assuming that one nucleus contains 6 pg of genomic DNA.

Results

Production of rAAVs with the insulator

Figure 1 shows the rAAV vector genomes constructed in the present study. We selected three insulators: DHS that had been found in a DNase I-hypersensitive site in the AAVS1 region, cHS4, and Ars, and inserted one of the insulators upstream of the promoter in the direction to insulate the luciferase expression cassette. AAVS1 on the q arm of human chromosome 19 is the specific target site of AAV2 for the integration of the viral genome. For comparison, Stuffer, an unrelated DNA fragment from the modified *Renilla* luciferase gene, was used in place of an insulator. We used four promoters: EF, CKM, CMV, and an enhancer-less version of CMV [CMV/E(−)], which lacks the enhancer region of CMV.

The rAAV was produced in the 293 FT cells transfected with the vector plasmid and the helper/packaging plasmid expressing the cap and rep genes of AAV2. The sizes of the vector genomes were in the range 3.66–4.60 kb. The rAAV was designated with the promoter and the insulator used for the construction of its vector genome. For example, rAAV having EF and DHS, CMV and cHS4, and CMV/E(−) and Stuffer were designated as rAAV-EF-DHS, rAAV-CMV-cHS4, and rAAV-CMV/E(−) -Stuffer, respectively. With our procedure, the level of each rAAV produced in a 10-cm culture plate was within the range from 3×10^8 to 5×10^8 genome copies, indicating that these insulators did not affect the packaging of the vector genome.

Transduction of mouse C2C12 cells, a myoblast cell line, with the rAAVs

The inserted DHS or cHS4 enhanced the transgene expression from EF in the C2C12 cells, a myoblast cell line derived from a C3H mouse. However, the insulators did not affect the transgene expression from CMV. The rAAV (1×10^8) was inoculated to the C2C12 cells and luciferase activity of the cell lysate was measured at 72 h after inoculation (Figure 2). The luciferase activities induced by rAAV-EF-DHS and rAAV-EF-cHS4 were two- to three-fold higher than those induced by rAAV-EF-Stuffer (Figure 2A). The luciferase activities induced by rAAV-CMV-DHS, rAAV-CMV-cHS4, and rAAV-CMV-Ars were similar to those induced by rAAV-CMV-Stuffer (Figure 2A). The luciferase activity induced by rAAV-CMV/E(−) was extremely low and was enhanced by the insertion of DHS to the level of 1 : 200 of rAAV-CMV-Stuffer (Figure 2B), indicating that DHS did not compensate the CMV enhancer. Thus, DHS and cHS4 raised the transgene-expression from EF to a level comparable to that induced from CMV, which is one of the most efficient promoter/enhancer systems.

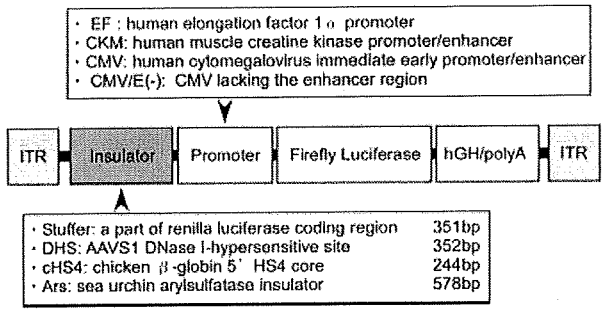

Figure 1. Schematic representation of rAAV genomes. ITR, inverted terminal repeat; hGH/pA, poly A site of human growth hormone gene

Transduction of the mouse muscle with the rAAVs

Figure 3A shows luciferase activities induced by rAAV-EFs in mice. The quadriceps muscle of 4-week-old female BALB/c mice was injected with 50 μl of the rAAV-EFs (1×10^8, 1×10^9 or 1×10^{10} genome copies) in PBS or plain PBS for the measurement of background. Each rAAV preparation was injected into five (in some cases, four or six) legs. The left and right legs were used for different rAAVs to reduce intermouse variability. The luciferase activity of the injected muscle was measured at 4 weeks after injection. Although, at a dose of 1×10^8 genome copies, luciferase activity induced by rAAV-EF-Stuffer was almost at the background level, luciferase activities induced by rAAV-EF-DHS and rAAV-EF-cHS4 were readily detectable. The luciferase levels increased depending on the doses. At all doses tested, the average

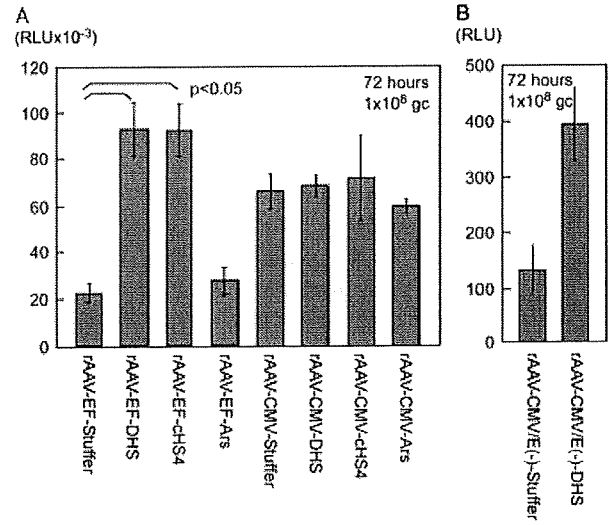

Figure 2. Transduction of C2C12 cells with (A) rAAV-EFs and rAAV-CMVs and (B) rAAV-CMV/E(−)s. C2C12 cells (1×10^4) were inoculated with the indicated rAAV and lysed 72 h later. The luciferase activity of the lysate was measured. The average of three independent experiments is presented with error bars indicating the standard deviation

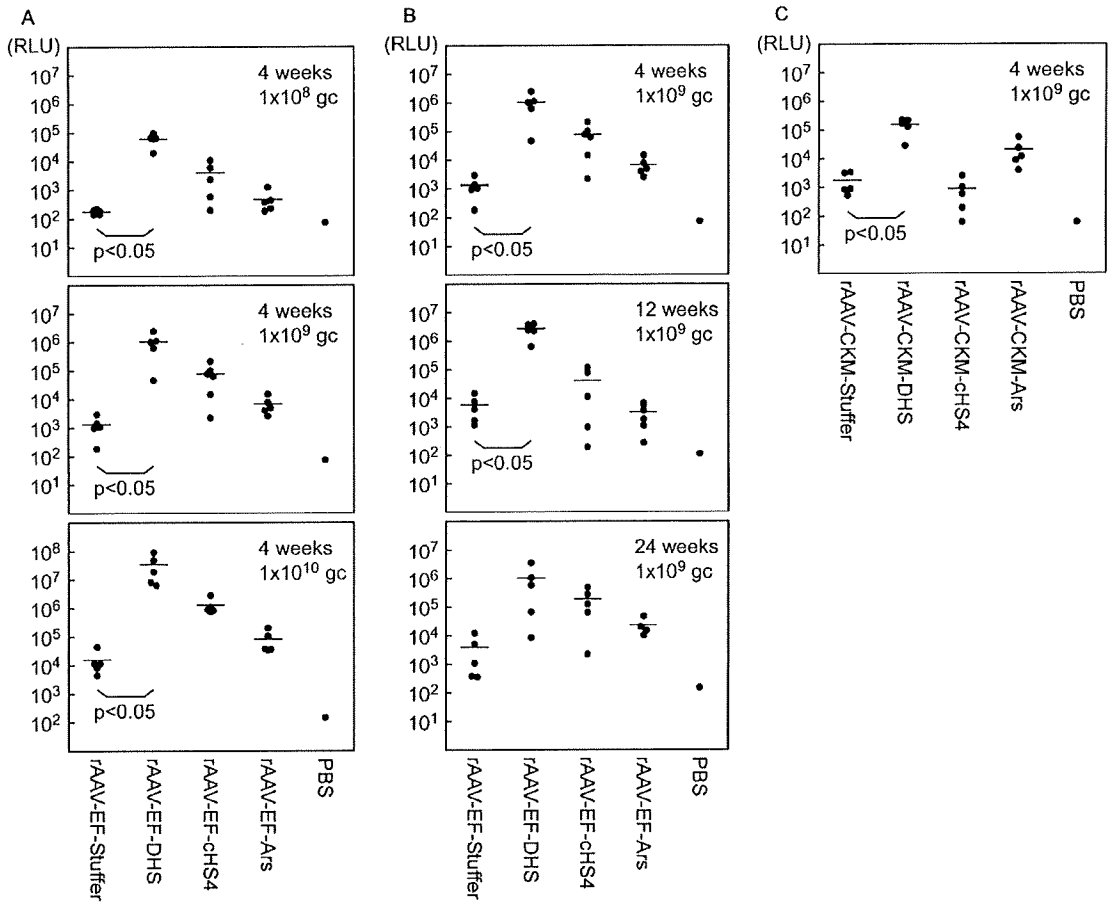

Figure 3. Transduction of the mouse muscle with rAAVs. (A) Levels of luciferase induced by various doses of rAAV-EFs. The mouse quadriceps muscle was inoculated with the indicated rAAV and harvested at 4 weeks after injection. The muscle was minced and lysed, and measured for luciferase activity. Bars indicate the average values. $p < 0.05$ (t-test) was considered statistically significant. (B) Levels of luciferase at 4, 12, and 24 weeks after injection with rAAV-EFs. The mouse quadriceps muscle inoculated with the indicated rAAV was harvested at 4, 12, and 24 weeks after injection. The luciferase activity was measured in a similar manner. Bars indicate the average values. $p < 0.05$ (t-test) was considered statistically significant. (C) Levels of luciferase induced by rAAV-CKMs. The mouse quadriceps muscle inoculated with the indicated rAAV was harvested at 4 weeks after injection. The luciferase activity was measured in a similar manner. Bars indicate the average values. $p < 0.05$ (t-test) was considered statistically significant

luciferase levels induced by rAAV-EF-DHS and rAAV-EF-cHS4 were 1000-fold and 100-fold higher, respectively, than that induced by rAAV-EF-Stuffer.

The luciferase activity of the mouse muscle injected with the rAAV-EFs of 1×10^9 genome copies was measured at 4, 12, and 24 weeks after injection (Figure 3B). The expression of luciferase continued for at least 24 weeks and the levels were maintained.

Figure 3C shows luciferase activities induced by rAAV-CKMs in mice. The mouse muscle was injected with one of rAAV-CKMs (1×10^9 genome copies) and luciferase activity was measured at 4 weeks after injection. The average of luciferase levels induced by rAAV-CKM-DHS was 100-fold higher than that induced by rAAV-CKM-Stuffer, indicating that DHS enhanced the transgene expression from CKM, similar to the expression from EF, in the mouse muscle.

The insulators did not affect transgene expression from CMV in the mouse muscle. The mouse muscle was injected with one of rAAV-CMVs (1×10^9 genome copies) and luciferase activity was measured at 4 weeks after injection. The luciferase level induced by rAAV-CMVs with insulator was similar to that by rAAV-CMV-Stuffer (Figure 4A). Similarly, the insulators did not affect transgene expression in the mouse muscle from the human ubiquitin C promoter, from which luciferase was induced to a level comparable to that from CMV (data not shown).

The luciferase activity of the muscle injected with rAAV-CMV/E(−)-DHS was slightly higher compared to muscle injected with rAAV-CMV/E(−)-Stuffer (Figure 4B).

To examine the transduction of tissues other than the muscle, rAAV-EFs or rAAV-CKMs (1×10^9 genome copies/250 µl of PBS) was injected to each mouse (five mice for each rAAV) through the tail vain. Because the previous study indicated that rAAVs injected through the tail vain are present mainly in the liver and spleen [24], the entire liver and spleen were harvested 4 weeks later and processed as performed for the quadriceps muscle. A low level of luciferase activity was detected only for

DOI: 10.1002/jgm

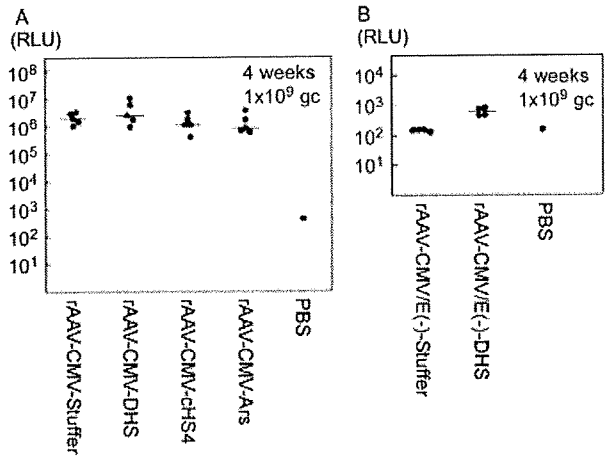

Figure 4. Transduction of the mouse muscle with (A) rAAV-CMVs and (B) rAAV-CMV/E(−) s. The mouse quadriceps muscle was inoculated with the indicated rAAV and harvested at 4 weeks after inoculation. The muscle was minced and lysed, and measured for luciferase activity. Bars indicate the average values

the liver of the mice injected with rAAV-EF-DHS (data not shown), suggesting that rAAV-EF-DHS transduced the liver more efficiently than the other rAAVs did.

Copy number of vector genome in the mouse muscle

The insulators did not affect copy number of the vector genome in the muscle. The rAAV-EFs (1×10^{10} genome copies) were injected to the quadriceps muscle in a similar manner and total DNA was extracted from the muscle at 4 weeks after injection. The level of the vector genome was measured by TaqMan PCR. Table 1 shows the calculated copy number of vector genome per nucleus. There was no significant difference between rAAV-EFs with the insulator and rAAV-EF-Stuffer. The data indicate that the enhanced luciferase activity of the muscle injected with rAAV-EF-DHS or rAAV-EF-cHS4 was not caused by a marked increase in the copy number of vector genome.

Effect of direction and location of DHS on the transduction enhancement

To determine whether or not the direction and location of DHS influence the DHS-mediated transduction enhancement, we constructed rAAV-EF-DHSs having DHS in the opposite direction or downstream of the luciferase gene and examined them for their transduction ability of mouse

Table 1. Copy number of vector genome in the mouse muscle

rAAV injected	Copy number of vector genome/nucleus	Average	SD
rAAV-EF-Stuffer	1.03, 0.76, 0.88, 0.49, 0.58	0.75	0.22
rAAV-EF-DHS	1.00, 1.16, 0.41, 2.65, 0.34	1.11	0.93
rAAV-EF-cHS4	2.39, 1.03, 7.28, 2.42, 0.84	2.79	2.62
rAAV-EF-Ars	1.75, 0.74, 0.87, 0.79, 0.22	0.87	0.55

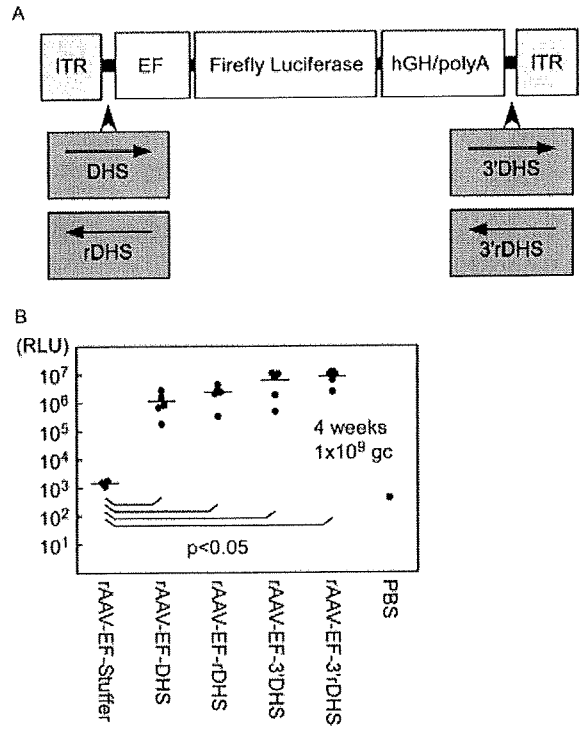

Figure 5. Transduction of the mouse muscle with rAAV-EFs having DHS in the opposite direction and downstream of the transgene. (A) Schematic representation of the various rAAV-EF-DHS genomes. ITR, inverted terminal repeat; rDHS, opposite direction to the transcription of the luciferase gene; hGH/pA, poly A site of human growth hormone gene; 3′DHS and 3′rDHS, DHS inserted downstream of the luciferase gene. (B) Levels of luciferase induced by the rAAV-EFs having DHS in the opposite direction and downstream of the transgene. The mouse quadriceps muscle was inoculated with the indicated rAAV and harvested at 4 weeks after inoculation. The muscle was minced and lysed, and measured for luciferase activity. Bars indicate the average values. $p < 0.05$ (t-test) was considered statistically significant

muscle. Figure 5A shows the structure of their vector genomes. The pAAV-EF1-Luc having DHS in the opposite direction was selected to produce rAAV-EF-rDHS. DHS was amplified by PCR with primers with an *Rsr*II site and inserted into the *Rsr*II site (between polyA signal and ITR) of pAAV-EF1-Luc to produce vector genomes for rAAV-EF-3′DHS and rAAV-EF-3′rDHS. These rAAVs were injected to the muscle in a similar manner, and luciferase activity of the muscle was measured 4 weeks later (Figure 5B). The luciferase activities induced by rAAV-EF-rDHS, rAAV-EF-3′DHS, and rAAV-EF-3′rDHS were comparable to that induced by rAAV-EF-DHS, indicating that the DHS-mediated enhancement does not depend on the direction or location of DHS in the AAV vector genome.

Discussion

In the present study, we newly constructed the rAAVs with selected insulators and examined their capability of transducing C2C12 cells and the mouse quadriceps

muscles. DHS and cHS4 raised the levels of transgene expression from EF by two- to three-fold in C2C12 cells and by 1000- and 100-fold, respectively, in the muscles. DHS also raised the levels of transgene expression from CKM by 100-fold in the muscles. Because the copy numbers of the vector genomes carrying the insulators in the mouse muscles were similar to those of the insulator-less genome, it is likely that the insulators enhanced the transcription from EF and CKM.

DHS did not enhance expression from CMV (one of the most efficient promoter/enhancer found so far) and the human ubiquitin C promoter. The data obtained suggest that DHS did not raise the presumed maximum level of transcription. Most likely, DHS enhances transcription from relatively less efficient promoters, EF and CKM. The transcriptional enhancing function of DHS, a 352 bp fragment, is likely to be useful for rAAV construction with a less efficient tissue specific promoter, such as CKM.

The molecular mechanism of the enhancement is not clear at present. Because previous studies clearly showed that the great majority of rAAV genomes are maintained as extrachromosomal concatemers of circular double-stranded DNA [5–7], DHS and cHS4 likely enhanced transcription of the transgene that was not integrated in cellular DNA. Although, in cellular DNA, the insulator sequences directionally act as boundaries to the surrounding heterochromatin that silences the genes located within [26], those in circular DNA (along with protein factors attached to DNA) may influence the entire chromatin structure of episomes. A possible structural change of the chromatin may account for the findings indicating that the insulator-mediated enhancement was independent of the direction and location of DHS in the AAV vector genome (Figure 5B). DHS inserted into the CMV/E(−) did not compensate the CMV enhancer, suggesting that the enhancing mechanism may be different from that of the classical enhancers. Further studies are required to determine how DHS enhances the transcription from the less efficient promoters.

Acknowledgements

We thank Dr Kunito Yoshiike for critical reading of the manuscript. This work was supported by Health and Labour Sciences Research Grants from the Ministry of Health, Labour and Welfare.

References

1. Flotte TR, Berns KI. Adeno-associated virus: a ubiquitous commensal of mammals. *Hum Gene Ther* 2005; **16**: 401–407.
2. Le Bec C AM. Douar AM. Gene therapy progress and prospects. Vectorology: design and production of expression cassettes in AAV vectors. *Gene Ther* 2006; **13**: 805–813.
3. Weitzman MD, Kyostio SR, Kotin RM, *et al.* Adeno-associated virus (AAV) Rep proteins mediate complex formation between AAV DNA and its integration site in human DNA. *Proc Natl Acad Sci USA* 1994; **91**: 5808–5812.
4. Giraud C, Winocour E, Berns KI. Recombinant junctions formed by site-specific integration of adeno-associated virus into an episome. *J Virol* 1995; **69**: 6917–6924.
5. Duan D, Sharma P, Yang J, *et al.* Circular intermediates of recombinant adeno-associated virus have defined structural characteristics responsible for long-term episomal persistence in muscle tissue. *J Virol* 1998; **72**: 8568–85772.
6. Vincent-Lacaze N, Snyder RO, Gluzman R, *et al.* Structure of adeno-associated virus vector DNA following transduction of the skeletal muscle. *J Virol* 1999; **73**: 1949–55.
7. Schnepp BC, Clark KR, Klemanski DL, *et al.* Genetic fate of recombinant adeno-associated virus vector genomes in muscle. *J Virol* 2003; **77**: 3495–3504.
8. Nakai H, Iwaki Y, Kay MA, *et al.* Isolation of recombinant adeno-associated virus vector-cellular DNA junctions from mouse liver. *J Virol* 1999; **73**: 5438–5447.
9. Flotte T, Carter B, Conrad C, *et al.* A phase I study of an adeno-associated virus-CFTR gene vector in adult CF patients with mild lung disease. *Hum Gene Ther* 1996; **7**: 1145–1159.
10. Kay MA, Manno CS, Ragni MV, *et al.* Evidence for gene transfer and expression of factor IX in haemophilia B patients treated with an AAV vector. *Nat Genet* 2000; **24**: 257–261.
11. Kaplitt MG, Feigin A, Tang C, *et al.* Safety and tolerability of gene therapy with an adeno-associated virus (AAV) borne GAD gene for Parkinson's disease: an open label, phase I trial. *Lancet* 2007; **369**: 2097–2105.
12. Bell AC, West AG, Felsenfeld G. Insulators and boundaries: versatile regulatory elements in the eukaryotic genome. *Science* 2001; **291**: 447–450.
13. Pikaart MJ, Recillas-Targa F, Felsenfeld G. Loss of transcriptional activity of a transgene is accompanied by DNA methylation and histone deacetylation and is prevented by insulators. *Genes Dev* 1998; **12**: 2852–2862.
14. Burgess-Beusse B, Farrell C, Gaszner M, *et al.* The insulation of genes from external enhancers and silencing chromatin. *Proc Natl Acad Sci USA* 2002; **99**(Suppl 4): 16433–16437.
15. Arumugam PI, Scholes J, Perelman N, *et al.* Improved human β-globin expression from self-inactivating lentiviral vectors carrying the chicken hypersensitive site-4 (cHS4) insulator element. *Mol Ther* 2007; **15**: 1863–1871.
16. Ma Y, Ramazani A, Lewis R, *et al.* High-level sustained transgene expression in human embryonic stem cells using lentiviral vectors. *Stem Cells* 2003; **21**: 111–117.
17. Ye X, Liang M, Meng X, *et al.* Insulation from viral transcriptional regulatory elements enables improvement to hepatoma-specific gene expression from adenovirus vectors. *Biochem Biophys Res Commun* 2003; **307**: 759–764.
18. Ramezani A, Hawley TS, Hawley RG. Performance and safety enhanced lentiviral vectors containing the human interferon-β scaffold attachment region and the chicken β-globin insulator. *Blood* 2003; **101**: 4714–4724.
19. Ogata T, Kozuka T, Kanda T. Identification of an insulator in AAVS1, a preferred region for integration of adeno-associated virus DNA. *J Virol* 2003; **77**: 9000–9007.
20. Recillas-Targa F, Pikaart MJ, Burgess-Beusse B, *et al.* Position-effect protection and enhancer blocking by the chicken β-globin insulator are separable activities. *Proc Natl Acad Sci USA* 2002; **99**: 6883–6888.
21. Akasaka K, Nishimura A, Tanaka K, *et al.* Upstream element of the sea urchin arylsulfatase gene serves as an insulator. *Cell Mol Biol* 1999; **45**: 555–565.
22. Boshart M, Weber F, Jahn G, *et al.* A very strong enhancer is located upstream of an immediate early gene of human cytomegalovirus. *Cell* 1985; **41**: 521–530.
23. Yaffe D, Saxel O. Serial passaging and differentiation of myogenic cells isolated from dystrophic mouse muscle. *Nature* 1977; **270**: 725–727.
24. Mori S, Wang L, Takeuchi T, Kanda T. Two novel adeno-associated viruses from cynomolgus monkey: pseudotyping characterization of capsid protein. *Virology* 2004; **330**: 375–383.
25. Auricchio A, Hildinger M, O'Connor E, *et al.* Isolation of highly infectious and pure adeno-associated virus type 2 vectors with a single-step gravity-flow column. *Hum Gene Ther* 2001; **12**: 71–76.
26. Burgess-Beusse B, Farrell C, Gaszner M, *et al.* The insulation of genes from external enhancers and silencing chromatin. *Proc Natl Acad Sci USA* 2002; **99**: 16433–16437.

Acta Oncologica, 2009; 48: 1193–1197

informa
healthcare

ORIGINAL ARTICLE

Quality assurance of volumetric modulated arc therapy using Elekta Synergy

AKIHIRO HAGA[1], KEIICHI NAKAGAWA[1], KENSHIRO SHIRAISHI[1], SAORI ITOH[1], ATSURO TERAHARA[1], HIDEOMI YAMASHITA[1], KUNI OHTOMO[1], SHIGEKI SAEGUSA[1], TOSHIKAZU IMAE[1], KIYOSHI YODA[2] & ROBERTO PELLEGRINI[3]

[1]*Department of Radiology, University of Tokyo Hospital, 7-3-1 Hongo, Bunkyo-ku, Tokyo 113-8655 Japan,* [2]*Elekta KK, Kobe, Japan and* [3]*Elekta, 30 Line, Milano, Italy*

Abstract

Purpose. Recently, Elekta has supplied volumetric modulated arc therapy (VMAT) in which multi-leaf collimator (MLC) shape, jaw position, collimator angle, and gantry speed vary continuously during gantry rotation. A quality assurance procedure for VMAT delivery is described. *Methods and materials.* A single-arc VMAT plan with 73 control points (CPs) and 5-degree gantry angle spacing for a prostate cancer patient has been created by ERGO++ treatment planning system (TPS), where MLC shapes are given by anatomic relationship between a target and organs at risk and the monitor unit for each CP is optimized based on given dose prescriptions. Actual leaf and jaw positions, gantry angles and dose rates during prostate VMAT delivery were recorded in every 0.25 seconds, and the errors between planned and actual values were evaluated. The dose re-calculation using these recorded data has been performed and compared with the original TPS plan using the gamma index. *Results.* Typical peak errors of gantry angles, leaf positions, and jaw positions were 3 degrees, 0.6 mm, and 1 mm, respectively. The dose distribution obtained by the TPS plan and the recalculated one agreed well under 2%-2 mm gamma index criteria. *Conclusions.* Quality assurance for prostate VMAT delivery has been performed with a satisfied result.

The concept of volumetric modulated arc therapy (VMAT) originated from the conformal avoidance radiation therapy [1] with a dynamical movement of MLC while rotating the gantry. By modulating beam intensity during the gantry rotation, intensity modulated arc therapy (IMAT) was proposed and further investigated [2–6]. VMAT is one of the techniques to realize IMAT by varying gantry speed and dose rate with dynamical movement of MLC and jaw [7]. Recently, this has been clinically available [8–10] and a combination of Elekta Synergy with the latest linac control software and ERGO++ treatment planning system (TPS) is one example.

The purpose of this paper is to investigate how much error is caused in dose distribution due to the fluctuation in the dynamical parameters. The linac controller in Elekta Synergy (Elekta, Crawley, UK), RT Desktop 7.0.1, serves to record measured data of dose rates, gantry angles, MLC and jaw positions with 0.25 s interval during VMAT treatment. We can evaluate the influence of these errors by recalculating the dose distribution with these actual dynamical parameters. Since this is an independent simulation analysis and therefore we may be able to specify the cause when VMAT film verification failed.

Methods and materials

A single-arc VMAT plan for prostate cancer was created by ERGO++ v1.71 TPS (Elekta/3DLine, Milano) with D95 prescription (dose to 95% of target volume) of 76 Gy in 38 fractions. A single arc was discretized into 73 static beams or CPs placed at 5-degree gantry angle intervals between −175 and +175 degrees and the first and last CPs were positioned at −179 and +179 degrees (Figure 1). The field shape for each control point was determined by either conformal or conformal avoidance strategy with a 6 mm leaf margin to Planning Target Volume (PTV). In other words, the rectum was

Correspondence: Akihiro Haga, Department of Radiology, University of Tokyo Hospital, 7-3-1 Hongo, Bunkyo-ku, Tokyo 113-8655 Japan. Tel: +81 3 5800 9002. Fax: +81 3 5800 8786. E-mail: haga-haga@umin.ac.jp

(Received 5 April 2009; accepted 30 May 2009)

print/ISSN 1651-226X online
341860903081905

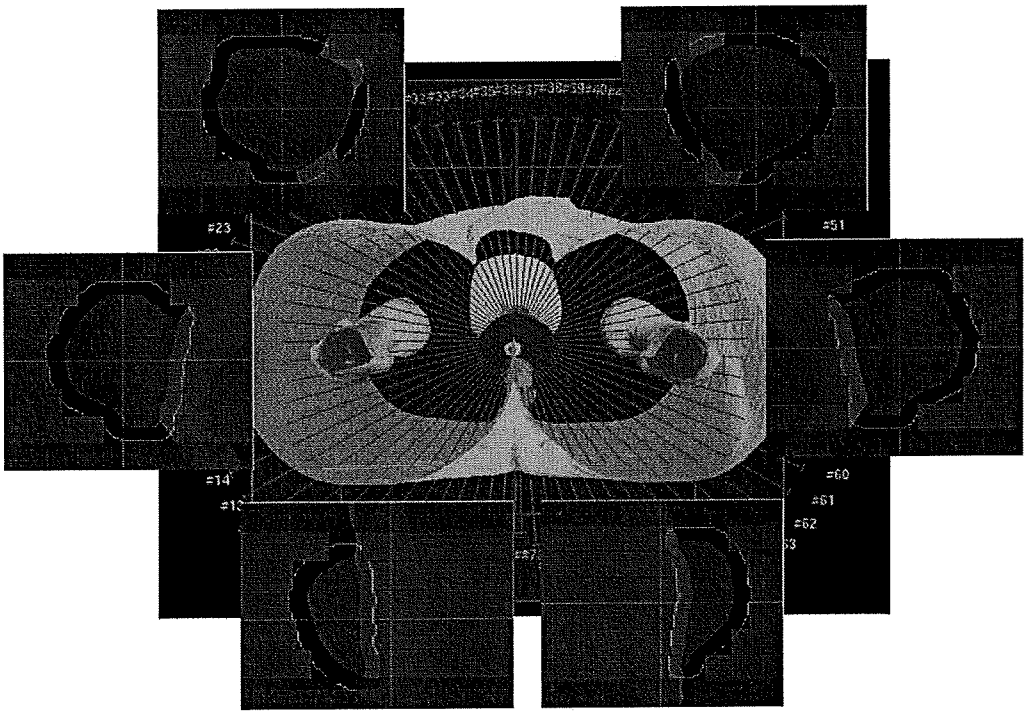

Figure 1. A single-arc VMAT plan with 73 CPs and 5-degree gantry angle spacing for a prostate cancer patient has been created by ERGO++ treatment planning system, where MLC shapes are given by anatomies of target and organs at risk and monitor units for each CP is optimized by simulated annealing algorithm based on given dose prescriptions. The red and pink regions are PTV and rectum, respectively.

partially shielded by MLC when it was in front of the target in beam's eye view, while the whole target was irradiated when it was in front of the rectum.

In the present study, the collimator angle was fixed at 180 degrees. Beam weights for all CPs were optimized by inverse planning based on the simulated annealing algorithm. Dose grid resolution was 2 mm × 2 mm × 2 mm for 3D calculation. After inverse planning, the CPs were grouped into a single arc with the VMAT sequencer in ERGO++ TPS, where a monitor unit (MU) to be delivered between two adjacent CPs was calculated by adding MUs at the two adjacent CPs and then multiplied by 0.5. The created plan was sent to MOSAIQ v1.6 (Elekta IMPAC, USA), and then delivered by the RT desktop controller.

For dose verification, VMAT plan was transferred to two phantom studies. One was a cylindrical water phantom with 0.015 cc pin-point ionization chamber (Type 31014, PTW, Germany) placed at the isocentre. The other was a pelvic water phantom including a GafChromic film (International Specialty Products, NJ, USA) to measure the dose distribution on axial, coronal, and sagittal planes including the isocentre. The GafChromic film was scanned using a flatbed scanner (EPSON GT-X770, Japan) and the gamma index with 3% of a dose at the measurement point and 3 mm has been evaluated by using DD-system v9.0 (R-tech, Japan).

The linac controller in service mode was capable of recording the actual gantry angle, MLC and jaw positions, and dose rate as a function of time. The MLC and jaw positions in each CP computed by ERGO++ were compared with the corresponding measured values. The cumulative MU error is practically negligible because Elekta VMAT delivery is based on MU-based servo control. Instead, the gantry angle error is discussed, which is defined as the difference between the gantry angle for each CP and the gantry angle where a cumulative MU reaches a specified value. A gantry speed dependence of these errors with the same VMAT plan was also examined by employing two times slower gantry speed than a commonly used clinical speed.

Using the actual data of gantry angle, MLC and jaw positions, and the cumulative MUs, dose distribution was re-calculated using Pinnacle v7.4i TPS (Philips, USA), and the dose in the original plan transferred into Pinnacle was compared with the re-calculated dose distribution.

Results

The beam-on time was typically 100 s for a single-arc prostate VMAT delivery. The isocentre dose discrepancy between plans and measurements for 17 patients was $-0.5 \pm 0.8\%$ (s.d.). The averages of the pass rate with a gamma criteria of 3 mm and 3% of a dose at the measurement point were 97.3%, 91.8%, and 92.2% on axial, sagittal, and coronal planes for a region having a dose greater than 30% of the isocentre dose, respectively.

Figure 2 demonstrates measured errors between planned and actual gantry angles during VMAT delivery for three consecutive runs. The red data points show the position errors for a normal delivery time of 100 s, whereas the blue data points show those for a delivery time of 200 s. The bar shows the error range for the three runs. The gantry angle ranges of zero gantry angle error were due to move-only control points with no dose delivery.

Figure 3a and b show measured errors between planned and actual leaf positions during VMAT delivery for three consecutive runs of the same VMAT plan as in Figure 2. Figure 3a depicts a position error of right leaf number 20, which is one of the centre leaves, whereas Figure 3b depicts a position error of left leaf number 20. Again the red data points show the position errors for a normal delivery time of 100 s, whereas the blue data points show those for a delivery time of 200 s. The bar shows the error range for the three runs. The gantry angle ranges of zero leaf error were due to move-only control points with no dose delivery.

Figure 4a and b depicts measured errors between planned and actual X1 and X2 back-up jaw positions, respectively, during VMAT delivery for three consecutive runs of the same VMAT plan. Once again, the red data points show the position errors for a normal delivery time of 100 s, whereas the blue data points show those for a delivery time of 200 s. The bar shows the error range for the three runs. The gantry angle ranges of zero back-up jaw error were due to move-only control points with no dose delivery.

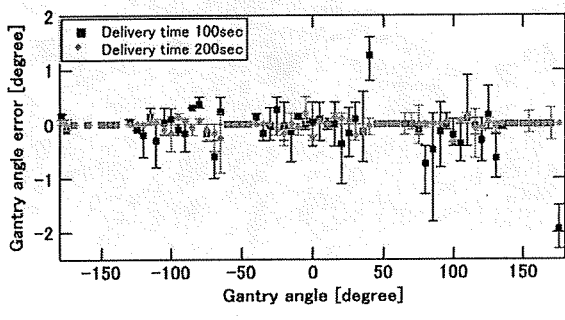

Figure 2. Measured errors between planned and actual gantry angles for three consecutive runs of the same VMAT plan. The red data points show the position errors for a normal delivery time of 100 s, whereas the blue data points show those for a delivery time of 200 s. The bar shows the error range for the three runs.

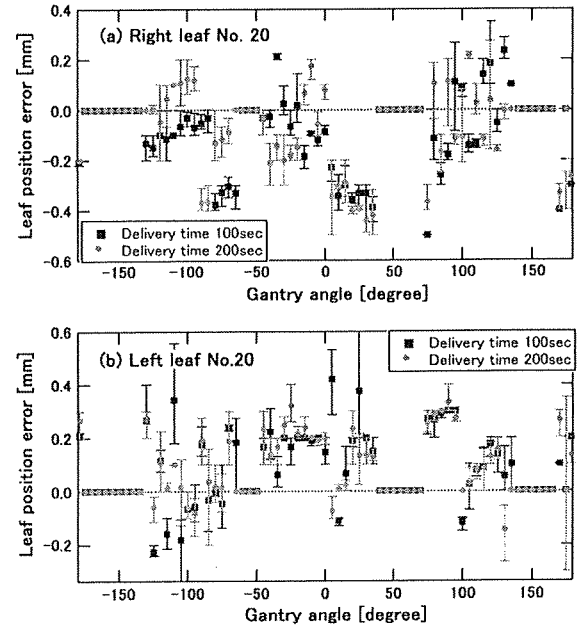

Figure 3. Measured errors between planned and actual leaf positions of the two centre leaves for three consecutive runs of the same VMAT plan: (a) position error of right leaf number 20, (b) position error of left leaf number 20. Again the red data points show the position errors for a normal delivery time of 100 s, whereas the blue data points show those for a delivery time of 200 s. The bar shows the error range for the three runs. The gantry angle ranges of zero leaf error were due to move-only control points with no dose delivery.

Figure 5a and b show gamma-index comparisons between an ERGO++ plan and re-calculated dose using actual data of MLC and jaw positions, gantry angles, and MUs with an interval of every 1 s. The red areas indicate gamma indices of larger than one under criteria of (a) 2% of a dose at the calculated point and 2 mm and (b) 1% of a dose at the calculated point and 1 mm.

Discussion

We have shown highly accurate prostate VMAT delivery using Elekta Synergy and ERGO++ TPS. While the dose agreement in the isocentre shows that total MU is correctly delivered, the agreement of dose distribution on axial, sagittal, and coronal planes assures accurate VMAT delivery. In the Synergy control system, the MLC, jaw, and gantry speed are servo-controlled based on cumulative MUs in each CP. Hence the errors in such dynamical parameters are quickly compensated by

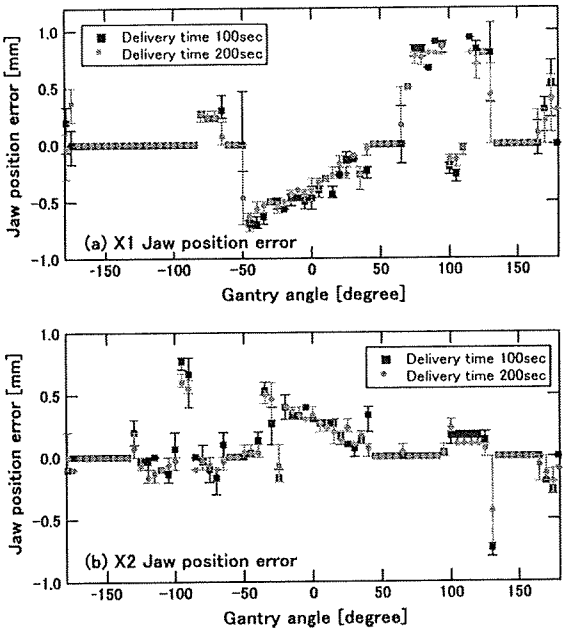

Figure 4. Measured errors between planned and actual back-up jaw positions for three consecutive runs of the same VMAT plan: (a) position error of X1 jaw, (b) position error of X2 jaw. Once again the red data points show the position errors for a normal delivery time of 100 s, whereas the blue data points show those for a delivery time of 200 s. The bar shows the error range for the three runs. The gantry angle ranges of zero back-up jaw error were due to move-only control points with no dose delivery.

real-time feedback control. For instance, it was found that the gantry angle error was immediately corrected as seen in Figure 2. In addition to the mechanical control, it is very important to mention that ERGO++ creates the MLC shape based on the anatomy relationship between the target and organs at risk from the beams eye view. Since it is a smooth function of gantry angle, no major changes are observed in MLC and jaw positions between adjacent control points thereby leading to more accurate dose calculation in TPS.

In the present work, the errors in gantry angles, MLC and jaw positions during VMAT delivery were analyzed. As seen in Figures 2–4, these errors were reproduced among three consecutive runs of the same VMAT plan, and were considered to be caused by accelerations of gantry, leaves, and jaws, which were required in almost the same gantry angles. In fact, it was clearly observed that the gantry angle error decreased when the gantry speed was slower as shown in Figure 2. In principle, smaller leaf and jaw position errors can be anticipated when the gantry speed is slower due to lower leaf and jaw speeds. In the present prostate plan which has no large leaf and jaw movements during gantry rotation, the leaf and back-up jaw position errors were comparable between two different delivery times. Instead, error tolerances of leaf and jaw positions given in the radiation control system may be a major cause of the observed errors.

As shown in Figure 5, the influence of these dynamical errors was negligible under criteria of 2% of a dose at the calculated point and 2 mm. Even under 1% of a dose at the calculated point and 1 mm criteria, the result was good except for low dose region. In other words, the errors in the dynamical parameters with the observed orders in prostate VMAT delivery do not affect the resulting dose distribution significantly.

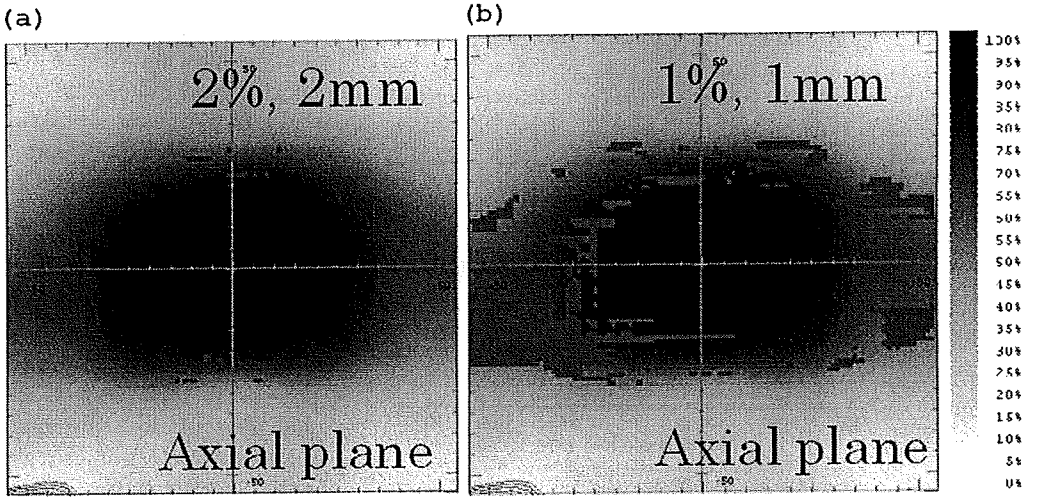

Figure 5. Gamma comparison between an ERGO++ plan and re-calculated dose using actual data of MLC and jaw positions, gantry angles, and MUs with an interval of every 1 s. The red areas indicate gamma indices of larger than one under criteria of (a) 2% of a dose at the calculated point and 2 mm and (b) 1% of a dose at the calculated point and 1 mm.

Conclusion

VMAT dose measurement for prostate cancer agreed well with the plan created by ERGO++. The observed errors of the dynamical parameter did not affect the dose distribution significantly. Quality assurance for prostate VMAT plans has been performed with a satisfied result.

Declaration of interest: Dr. Nakagawa receives research funding from Elekta KK.

References

[1] Takahashi S. Conformation radiotherapy: Rotation techniques as applied to radiography and radiotherapy of cancer. Acta Radiol Suppl 1965;242:1–142.

[2] Yu CX. Intensity-modulated arc therapy with dynamic multileaf collimation: An alternative to tomotherapy. Phys Mod Biol 1995;40:1435–49.

[3] Yu CX, Li XA, Ma I, et al. Clinical implementation of intensity modulated arc therapy. Int J Radiat Oncol Biol Phys 2002;53:453–6.

[4] Earl MA, Shepard DM, Maqvi SA, et al. Intensity modulated arc therapy simplified. Int J Radiat Oncol Biol Phys 2002;53:222–35.

[5] Earl MA, Shepard DM, Maqvi SA, et al. Inverse planning for intensity modulated arc therapy using direct aperture optimization. Phys Med Biol 2003;48:1075–89.

[6] Shepard DM, Cao D, Afghan MKN, Earl MA. An arc-sequencing algorithm for intensity modulated arc therapy. Med Phys 2007;34:464–70.

[7] Otto K. Volumetric modulated arc therapy: IMRT in a single gantry arc. Med Phys 2008;35:310–7.

[8] Bedford JL, Nordmark HV, MacNair HA, Aitken AH, Brock JE, et al. Treatment of lung cancer using volumetric modulated arc therapy and image guidance: A case study. Acta Oncol 2008;47:1438–43.

[9] Bedford JL, Warrington AP. Commissioning of volumetric modulated arc therapy (VMAT). Int J Radiat Oncol Biol Phys 2009;73:537–45.

[10] Korrenman S, Medin J, Kristoffersen FK. Dosimetric verification of RapidArc treatment delivery. Acta Oncol 2009;48:185–91.

Neurol Med Chir (Tokyo) 49, 456～461, 2009

Stereotactic Radiosurgery for Skull Base Meningioma

Hiroshi IGAKI*,**, Keisuke MARUYAMA***, Tomoyuki KOGA***, Naoya MURAKAMI**, Masao TAGO**,†, Atsuro TERAHARA**, Masahiro SHIN***, Keiichi NAKAGAWA**, and Kuni OHTOMO**

*Department of Radiology, Teikyo University School of Medicine, Tokyo; Departments of **Radiology and ***Neurosurgery, The University of Tokyo Hospital, Tokyo; †Department of Radiology, Toho University Omori Medical Center, Tokyo

Abstract

Stereotactic radiosurgery is now a treatment option for meningiomas, especially for high-risk patients such as those with skull base lesions. The clinical outcomes were retrospectively analyzed of stereotactic radiosurgery using the Leksell Gamma Knife® performed for 98 patients with 106 skull base meningiomas at the University of Tokyo Hospital between June 1990 and April 2006 and followed up for more than a year. After a median follow-up period of 53.2 months (range 12.2–204.4 months), local tumor control rates were 86.9% and 78.9% at 5 years and 10 years, respectively. Tumors with volume of 4 cm^3 or smaller (97.5% vs. 76.1% at 5 years, p = 0.001) and tumors completely included within the isodose line of 14 Gy or more (97.5% vs. 67.2% at 5 years, p = 0.0006) had higher local control rates. Postoperative residual tumors treated by stereotactic radiosurgery were controlled in all 25 cases. Cranial nerve deficits were improved, stable, and deteriorated in 12, 64, and 3 patients, respectively, after stereotactic radiosurgery. Stereotactic radiosurgery was effective treatment method for local control of skull base meningiomas, especially for small or postoperative residual tumors. Correct combination of microsurgery and radiosurgery leads to excellent local control.

Key words: gamma knife, skull base, meningioma, stereotactic radiosurgery, local control

Introduction

Meningioma is the most common type of intracranial tumor arising from the meninges, with an incidence of 4.5 per 100,000 person-years, and accounts for 30.1% of all primary brain and central nervous system tumors.[3] The standard treatment for meningioma is surgical resection through craniotomy, targeted at gross total removal.[2,4,6,9,16,23,24,31,35] The treatment goal is long-term tumor control with minimal neurological morbidity. However, the tumor often extends to important neurovascular structures in the skull base, so total tumor resection (Simpson grades 1–2) is achieved in only 20–87.5% of patients.[2,4,23,24,31,35] Unacceptably high incidences of symptomatic recurrence are observed after subtotal resection of meningiomas.[20,33] In addition, postoperative complications occur in 16.1–61.5% of patients, although overall complication rates are not always reported.[2,23,31,35]

Stereotactic radiosurgery has now become a less invasive and effective treatment option for intracranial meningioma, especially in patients with high-risk tumors such as skull base lesions.[1,11–16,18,19,21,22,26,27,30,32,34,37] Stereotactic radiosurgery provides excellent outcomes with local tumor control rates of 85–100%, but these rates tend to fall with longer follow-up periods.[11–15,18,19,21,26,27,30,32,34] However, recent local tumor control rates have been nearly 100% for patients who had undergone Simpson grade 1 surgery.[16,28] Therefore, correct combination of microsurgery and radiosurgery would seem to have attained better clinical results with cavernous sinus meningiomas in our earlier series and in other institutions.[5,7,10,17,19,25] The Leksell Gamma Knife® (Elekta Instruments AB, Stockholm, Sweden) was installed in 1990 at the University of Tokyo Hospital. Since then, we have treated patients with intracranial tumors by stereotactic radiosurgery as a single modality treatment or in combination with surgery.

This study retrospectively reviewed the outcomes of stereotactic radiosurgery for skull base meningioma at the University of Tokyo Hospital and analyzed the factors affecting the results.

Received January 20, 2009; Accepted March 23, 2009

Materials and Methods

Ninety-eight patients with 106 skull base meningiomas were treated by stereotactic radiosurgery, twice in 6 patients and three times in one patient, at the University of Tokyo Hospital and followed up for more than a year between June 1990 and April 2006. The clinical courses and treatment outcomes were retrospectively analyzed (Table 1).

Written informed consent was obtained from the patients before treatment. The patients were immobilized with a Leksell stereotactic coordinating frame and underwent high-resolution stereotactic magnetic resonance (MR) imaging or computed tomography (CT). The treatment plan was based on the stereotactic images processed with commercially available software (KULA or GammaPlan; Elekta Instruments AB). The tumor was generally covered with the 40–50% isodose line, and the designated treatment dose (ideally 14 to 18 Gy) was delivered to the tumor margin.

The patients were followed up to monitor local tumor control, survival, and neurological status at our hospitals or by the referring physicians. Neurological evaluations and MR imaging were performed 3, 6, and 12 months after stereotactic radiosurgery, then every 6 months for the next 2 years, and annually thereafter. Follow-up and survival periods were calculated from the day of stereotactic radiosurgery. Actuarial local control and survival rates were calculated by the Kaplan-Meier method from the day of stereotactic radiosurgery. Local control was defined as free from local tumor regrowth after stereotactic radiosurgery as evaluated by MR imaging. The differences between groups was assessed with the log-rank test. Differences were considered statistically significant if $p < 0.05$.

Table 1 Patients' and disease characteristics

Features	Value
Age at treatment (yrs)	
range	16–76
median	52
Male:female	21:77
Tumor location	
cavernous sinus	48
petroclival	29
cerebellopontine angle	11
orbit	6
others	12
Treatment settings	
post-biopsy	2
postoperative residual	25
postoperative recurrence	39
definitive GKS	35
post-GKS recurrence	3
post(operation + GKS) recurrence	2
Tumor volume (cm^3)	
range	0.3–45.0
median	3.9
Dose to the tumor margin (Gy)	
range	12–22.5
median	16
Pathological diagnosis	
meningothelial	58
fibrous	6
transitional	2
atypical	2
meningioma, NOS	1
no pathology	37

GKS: gamma knife surgery, NOS: not others specified.

Results

Local tumor progression was observed in 15 patients after a median follow-up period of 53.2 months (range 12.2–204.4 months) after stereotactic radiosurgery. Actuarial local tumor control rates were 86.9% and 78.9% at 5 years and 10 years, respectively (Fig. 1). The tumors with volume of 4 cm^3 or smaller had a higher local control rate than those with volume of larger than 4 cm^3 (97.5% vs. 76.1% at 5 years, $p = 0.001$) (Fig. 2A). Local control rates were also better in tumors with the entire volume included within the isodose line of 14 Gy or more than tumors with incomplete coverage by the 14 Gy isodose line (97.5% vs. 67.2% at 5 years, $p = 0.0006$) (Fig. 2B). Treatment dose at the tumor margin and stereotactic images used for treatment planning did not influence local tumor control (90.9% for doses higher than 16 Gy vs. 85.3% for doses of 16 Gy or lower at 5 years, $p = 0.41$; 88.0% by MR imaging vs. 85.3% by CT at 5 years, $p = 0.99$) (Fig. 3). Postoperative residual tumors treated with stereotactic radiosurgery as an adjuvant modality were controlled in all 25 cases, but the local control rate of the

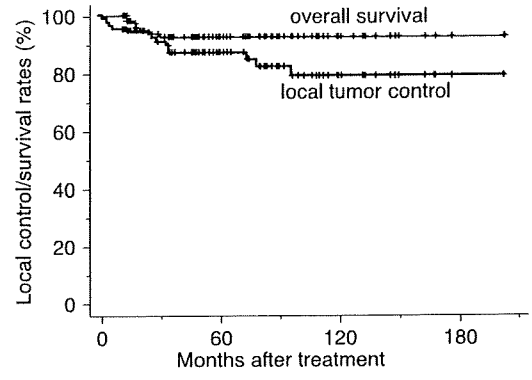

Fig. 1 Kaplan-Meier estimates of actuarial local tumor control and survival rates for all patients.

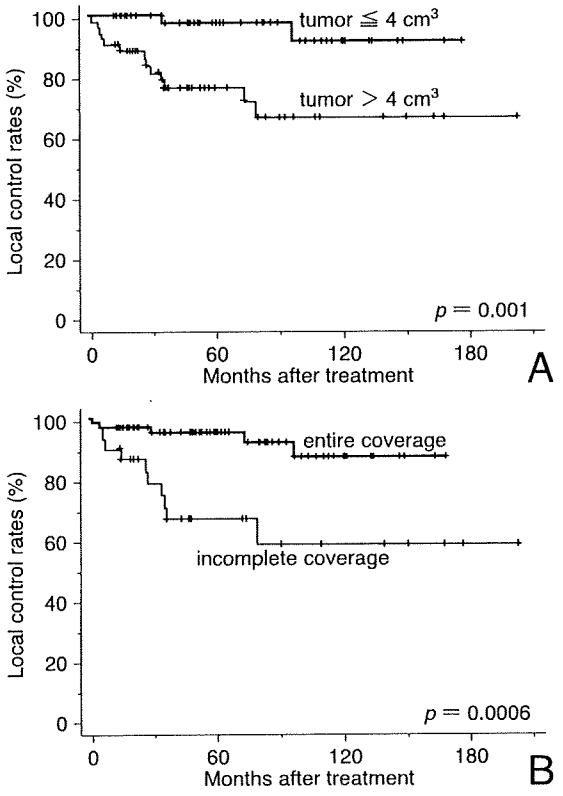

Fig. 2 **Kaplan-Meier estimates of actuarial local tumor control rates by tumor volume (A) and tumor coverage at treatment (B) showing significant differences.**

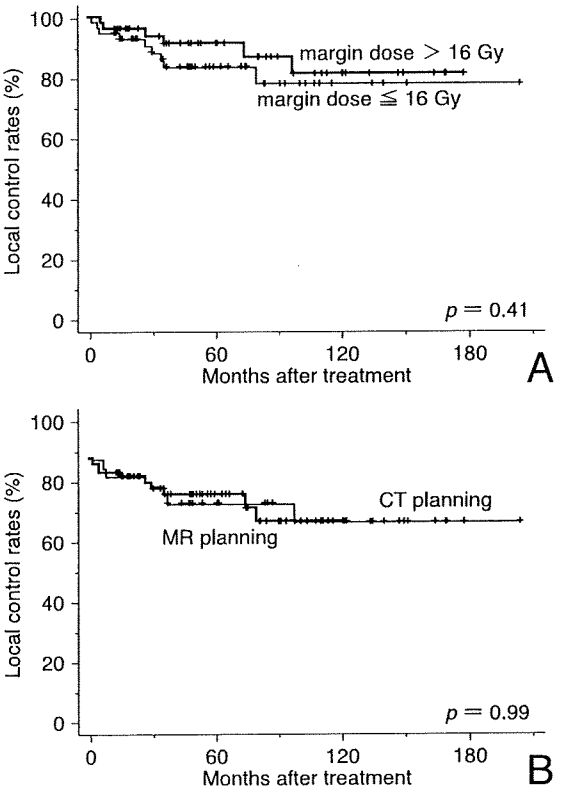

Fig. 3 **Kaplan-Meier estimates of actuarial local tumor control rates by margin dose (A) and treatment planning method (B) showing no significant differences. CT: computed tomography, MR: magnetic resonance.**

recurrent and untreated tumors treated with only stereotactic radiosurgery was 89.7% and 75.5% at 5 years, respectively, which was apparently inferior to the local control rate of 100% achieved by the two-staged strategy (Fig. 4). Overall survival rates were 92.5% and 92.5% at 5 years and 10 years, respectively (Fig. 1).

Eighty patients had cranial nerve deficits before stereotactic radiosurgery. Improvement was observed in 12 patients and worsening of the symptoms present at the treatment in 2 patients after the treatment. Cranial nerve deficits remained stable in the other 66 patients. Newly developed permanent radiation-induced cranial nerve deficits were noted in one patient after stereotactic radiosurgery. Cranial nerve functions are summarized in Table 2.

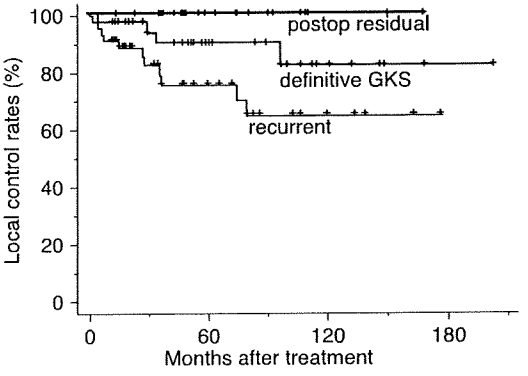

Fig. 4 **Kaplan-Meier estimates of actuarial local tumor control rates by treatment setting. GKS: gamma knife surgery.**

Discussion

The present study showed that tumor volume of 4 cm³ or smaller and complete tumor coverage were associated with better local control (Fig. 2). In addition, local control was apparently superior in the patients treated by stereotactic radiosurgery for postoperative residual tumor compared to treatment for recurrent tumor or single modality stereotactic radiosurgery treatment (Fig. 4). This difference presumably reflected the tumor debulking by surgical intervention before stereotactic radiosurgery, resulting in the beneficial condition of smaller tumor volume at the time of stereotactic radiosur-

Table 2 Cranial nerve function after gamma knife surgery (GKS)

Cranial nerves	Symptomatic before GKS	Improved	Worsened**	Transient deficits***	Permanent deficits***
I	1	0	0	0	0
II	24	1	1	0	0
III	21	3	0	0	0
IV	19	2	0	0	0
V	42	7	1	3	0
VI	33	8	0	0	0
VII	10	1	0	0	1
VIII	25	2	0	0	0
IX	2	0	0	0	1
X	2	0	0	0	1
XI	0	0	0	0	0
XII	1	0	0	0	0
All	80	12*	2	3	1

*Improvement of at least one cranial nerve symptom with no worsening of any cranial nerve symptom. **Deterioration of symptom which had been observed before GKS. ***New development of symptom which had not existed before GKS.

gery.

Local control rates showed no significant difference between patients treated by MR imaging-based planning and by CT-based planning (Fig. 3B). Tumor volume delineated by MR imaging is known to differ considerably from that by CT.[29] In addition, MR imaging has a problem of image distortion, which can influence the setup error.[36] However, the stereotactic images used in the treatment planning did not affect the local tumor control in our experience, or in previous similar findings.[8]

The crude post-radiosurgical permanent complication rate of 3% (3/98 patients, Table 2) was not negligible, and longer follow-up periods might reveal higher complication rates, but our experience with skull base meningiomas was similar to that of other institutions. The median margin dose of 16 Gy was higher than that used at other institutions. We selected higher doses for skull base meningioma treatment because of the probable miserable consequences for local recurrence after stereotactic radiosurgery. Lower treatment dose is associated with reduced incidence of radiation-induced morbidities after stereotactic radiosurgery, and some investigators reported no influence on local tumor control.[11,22]

Local tumor control rates for skull base meningiomas after stereotactic radiosurgery were better in the patients with tumor volumes of 4 cm^3 or smaller, and the patients treated with adjuvant stereotactic radiosurgery for postoperative residual tumors. If the volume of the skull base meningioma is 4 cm^3 or smaller, the tumor can be treated by single modality stereotactic radiosurgery with good local control rate. If the tumor volume is larger than 4 cm^3, combined microsurgery and postoperative stereotactic radiosurgery is required if any residual tumor is detected postoperatively. Correct combination of the two modalities leads to excellent local tumor control.

References

1) Aichholzer M, Bertalanffy A, Dietrich W, Roessler K, Pfisterer W, Ungersboeck K, Heimberger K, Kitz K: Gamma knife radiosurgery of skull base meningiomas. *Acta Neurochir (Wien)* 142: 647-652, 2000
2) Bassiouni H, Asgari S, Stolke D: Tuberculum sellae meningiomas: functional outcome in a consecutive series treated microsurgically. *Surg Neurol* 66: 37-44, 2006
3) Central Brain Tumor Registry of the United States: 2005-2006 Primary Brain Tumors in the United States Statistical Report, 1998-2002 Years Data Collected. Hinsdale, Ill, Central Brain Tumor Registry of the United States, 2006 (accessed 2009 Jan 14). Available from: http://www.cbtrus.org/reports//2005-2006/2006report.pdf
4) Chi JH, McDermott MW: Tuberculum sellae meningiomas. *Neurosurg Focus* 14(6): e6, 2003
5) Davidson L, Fishback D, Russin JJ, Weiss MH, Yu C, Pagnini PG, Zelman V, Apuzzo ML, Giannotta SL: Postoperative Gamma Knife surgery for benign meningiomas of the cranial base. *Neurosurg Focus* 23(4): E6, 2007
6) De Monte F: Current management of meningiomas. *Oncology (Williston Park)* 9: 83-91, 96, 99-101, 1995
7) Duma CM, Lunsford LD, Kondziolka D, Harsh GR 4th, Flickinger JC: Stereotactic radiosurgery of cavernous sinus meningiomas as an addition or alternative to microsurgery. *Neurosurgery* 32: 699-705, 1993
8) Flickinger JC, Kondziolka D, Pollock BE, Lunsford LD: Evolution in technique for vestibular schwannoma radiosurgery and effect on outcome. *Int J Radiat Oncol Biol Phys* 36: 275-280, 1996
9) Goldsmith B, McDermott MW: Meningioma. *Neurosurg Clin N Am* 17: 111-120, vi, 2006

10) Iwai Y, Yamanaka K, Nakajima H: The treatment of skull base meningiomas — combining surgery and radiosurgery. *J Clin Neurosci* 8: 528–533, 2001
11) Iwai Y, Yamanaka K, Yasui T, Komiyama M, Nishikawa M, Nakajima H, Kishi H: Gamma knife surgery for skull base meningiomas. The effectiveness of low-dose treatment. *Surg Neurol* 52: 40–44, 1999
12) Kollová A, Liscák R, Novotný J Jr, Vladyka V, Simonová G, Janousková L: Gamma Knife surgery for benign meningioma. *J Neurosurg* 107: 325–336, 2007
13) Kreil W, Luggin J, Fuchs I, Weigl V, Eustacchio S, Papaefthymiou G: Long term experience of gamma knife radiosurgery for benign skull base meningiomas. *J Neurol Neurosurg Psychiatry* 76: 1425–1430, 2005
14) Lee JY, Kondziolka D, Flickinger JC, Lunsford LD: Radiosurgery for intracranial meningiomas. *Prog Neurol Surg* 20: 142–149, 2007
15) Lee JY, Niranjan A, McInerney J, Kondziolka D, Flickinger JC, Lunsford LD: Stereotactic radiosurgery providing long-term tumor control of cavernous sinus meningiomas. *J Neurosurg* 97: 65–72, 2002
16) Linskey ME, Davis SA, Ratanatharathorn V: Relative roles of microsurgery and stereotactic radiosurgery for the treatment of patients with cranial meningiomas: a single-surgeon 4-year integrated experience with both modalities. *J Neurosurg* 102 Suppl: 59–70, 2005
17) Lunsford LD: Contemporary management of meningiomas: radiation therapy as an adjuvant and radiosurgery as an alternative to surgical removal? *J Neurosurg* 80: 187–190, 1994
18) Malik I, Rowe JG, Walton L, Radatz MW, Kemeny AA: The use of stereotactic radiosurgery in the management of meningiomas. *Br J Neurosurg* 19: 13–20, 2005
19) Maruyama K, Shin M, Kurita H, Kawahara N, Morita A, Kirino T: Proposed treatment strategy for cavernous sinus meningiomas: a prospective study. *Neurosurgery* 55: 1068–1075, 2004
20) Mathiesen T, Lindquist C, Kihlstrom L, Karlsson B: Recurrence of cranial base meningiomas. *Neurosurgery* 39: 2–9, 1996
21) Morita A, Coffey RJ, Foote RL, Schiff D, Gorman D: Risk of injury to cranial nerves after gamma knife radiosurgery for skull base meningiomas: experience in 88 patients. *J Neurosurg* 90: 42–49, 1999
22) Nakaya K, Hayashi M, Nakamura S, Atsuchi S, Sato H, Ochial T, Yamamoto M, Izawa M, Hori T, Takakura K: Low-dose radiosurgery for meningiomas. *Stereotact Funct Neurosurg* 72 Suppl 1: 67–72, 1999
23) O'Sullivan MG, van Loveren HR, Tew JM Jr: The surgical resectability of meningiomas of the cavernous sinus. *Neurosurgery* 40: 238–247, 1997
24) Otani N, Muroi C, Yano H, Khan N, Pangalu A, Yonekawa Y: Surgical management of tuberculum sellae meningioma: role of selective extradural anterior clinoidectomy. *Br J Neurosurg* 20: 129–138, 2006
25) Pendl G, Schrottner O, Eustacchio S, Ganz JC, Feichtinger K: Cavernous sinus meningiomas — what is the strategy: upfront or adjuvant gamma knife surgery? *Stereotact Funct Neurosurg* 70 Suppl 1: 33–40, 1998
26) Pollock BE, Stafford SL: Results of stereotactic radiosurgery for patients with imaging defined cavernous sinus meningiomas. *Int J Radiat Oncol Biol Phys* 62: 1427–1431, 2005
27) Pollock BE, Stafford SL, Link MJ: Gamma knife radiosurgery for skull base meningiomas. *Neurosurg Clin N Am* 11: 659–666, 2000
28) Pollock BE, Stafford SL, Utter A, Giannini C, Schreiner SA: Stereotactic radiosurgery provides equivalent tumor control to Simpson Grade 1 resection for patients with small- to medium-size meningiomas. *Int J Radiat Oncol Biol Phys* 55: 1000–1005, 2003
29) Prabhakar R, Haresh KP, Ganesh T, Joshi RC, Julka PK, Rath GK: Comparison of computed tomography and magnetic resonance based target volume in brain tumors. *J Cancer Res Ther* 3: 121–123, 2007
30) Roche PH, Pellet W, Fuentes S, Thomassin JM, Regis J: Gamma knife radiosurgical management of petroclival meningiomas results and indications. *Acta Neurochir (Wien)* 145: 883–888, 2003
31) Sanna M, Bacciu A, Falcioni M, Taibah A, Piazza P: Surgical management of jugular foramen meningiomas: a series of 13 cases and review of the literature. *Laryngoscope* 117: 1710–1719, 2007
32) Shin M, Kurita H, Sasaki T, Kawamoto S, Tago M, Kawahara N, Morita A, Ueki K, Kirino T: Analysis of treatment outcome after stereotactic radiosurgery for cavernous sinus meningiomas. *J Neurosurg* 95: 435–439, 2001
33) Simpson D: The recurrence of intracranial meningiomas after surgical treatment. *J Neurol Neurosurg Psychiatry* 20: 22–39, 1957
34) Subach BR, Lunsford LD, Kondziolka D, Maitz AH, Flickinger JC: Management of petroclival meningiomas by stereotactic radiosurgery. *Neurosurgery* 42: 437–445, 1998
35) Voss NF, Vrionis FD, Heilman CB, Robertson JH: Meningiomas of the cerebellopontine angle. *Surg Neurol* 53: 439–446, 2000
36) Watanabe Y, Perera GM, Mooij RB: Image distortion in MRI-based polymer gel dosimetry of gamma knife stereotactic radiosurgery systems. *Med Phys* 29: 797–802, 2002
37) Zachenhofer I, Wolfsberger S, Aichholzer M, Bertalanffy A, Roessler K, Kitz K, Knosp E: Gamma-knife radiosurgery for cranial base meningiomas: experience of tumor control, clinical course, and morbidity in a follow-up of more than 8 years. *Neurosurgery* 58: 28–36, 2006

Address reprint request to: Hiroshi Igaki, M.D., Department of Radiology, Teikyo University School of Medicine, 2-11-1 Kaga, Itabashi-ku, Tokyo 173-8606, Japan.
e-mail: igaki-tky@umin.ac.jp

Commentary

This is a well presented and statistically sound article. Its merit lies in showing the usefulness of heightened radiation primarily or as supplemental treatment to microsurgery for skull base meningiomas. Base of Skull Surgery (BOSS) is an evolving discipline towards which this article does make a contribution. Although

suggested by the authors that skull base meningiomas even up to the size of 4 cm^2 can or should be treated by radiation treatment, it has to be clearly understood by neurosurgeons that surgery is superior and better for all tumors, from scalp to sole, including meningiomas. It is only in cases where surgery is not possible or is dangerous beyond reasonable limits, radiation may be used as a primary 'palliative' form of treatment.[1] Despite the success obtained by the authors, in recurrent or residual tumors, the role of radiation treatment for skull base meningiomas can at best be considered to be still under evaluation. It needs to be appreciated that the so-called base of the skull is fill-in-the-gap osseation between a jungle of neurovascular structures that traverse to-and-from the brain. All neurovascular structures are too precious to be trifled with by any radiation. Radiation offers short-term gain but spawns long-term, obstinate side-effects. One might summarize that anticytotic therapy (chemotherapy, radiotherapy) shall only be reserved for sites inaccessible to the knife.

Reference

1) Kothari M, Goel A: Anticytotics — Radiopalliation/chemopalliation and neuraxial neoplasms. Neurol India 56: 113–115, 2008

Atul GOEL, M.D.
Department of Neurosurgery
King Edward VII Memorial Hospital
& Seth G.S. Medical College
Parel, Mumbai, India

Igaki et al. have presented their results of stereotactic radiosurgery for skull base meningioma. Their overall results are good. Actual local tumor control rates were 86.5% and 78.9% at 5 years and 10 years, respectively, which are acceptable. The crude post-radiosurgical permanent complication rate was 3% (3/98 patients). More detailed analysis of cranial nerve complications is recommended, such as delineation of cranial nerves under the special MRI-based planning. Did any differences in these tumor control results depend on the pathological diagnosis (MIB-1 index)? Local control rates showed no significant difference between patients treated by MRI-based planning and by CT-based planning. How was the tumor margin covered, the so-called dural tail sign on MRI?

Masahiro IZAWA, M.D.
Department of Neurosurgery
Tokyo Women's Medical University
Tokyo, Japan

In this report, Igaki and his coauthors report the outcomes for stereotactic radiosurgery (SRS) using the gamma knife technology for a series of 98 patients with 106 skull-base meningiomas treated during a six-year interval. The minimum follow-up was one year. The authors, working in a center of excellence, have defined outcomes which can be related to several potential radiosurgical features. First, they found that long-term tumor control was enhanced when smaller volume tumors were used. Providing that there was no confounding dose selection effect, it is clear that smaller tumors, perhaps treated earlier in their clinical course, may offer patients superior results.

The authors confirm that minimal tumor coverage of the entire imaging-defined volume with 14 Gy is effective in achieving tumor control rates of more than 90% of patients. Their usual prescription dose was somewhat higher than most centers currently use (16 Gy at the margin), a dose selected because of their concern that treatment failure would be higher in patients who received a lower margin dose. However, they could not confirm any better tumor control rates with lower doses than 16 Gy at the margin. The authors also note that there seems to be little difference between the tumor control rate based on CT planning versus patients who had MRI-based planning. Of interest, the patients who did best represent those who had initial tumor debulking, after which the gamma knife was used as adjuvant management for the residual tumor. The patients who did least well were those who were treated in a delayed fashion after evidence of tumor recurrence or progression was noted. We have found that early post microsurgical SRS for postoperative residuals also improves tumor control rates.

The goal of radiosurgery has been to improve long-term tumor control and survival, and to reduce cranial nerve and other neurologic morbidity associated with aggressive surgical removal. I believe that the doses used at the edge are probably higher than necessary to achieve the same long-term tumor control rates, based on our cumulative experience in more than 3000 skull base cases. If one uses a rule of thumb that 13 Gy at the edge of a tumor (its margin) is radiobiologically equivalent to giving 52 Gy fractionated radiation therapy, then one can expect tumor control rates in the range of 90% at five years. The great advantage, of course, of radiosurgery is precision, accuracy, a single-day procedure treatment, integration of the planning and radiosurgical dose delivery in a single session, and excellent long-term reports of outcomes from many world-wide sites. The adverse radiation effect risk was extremely low, perhaps 1% of patients.

Long-term follow-up continues, as it needs to, for patients undergoing total microsurgical removal as well. However, multicenter experience now over more than 25 years indicates that radiosurgery of skull-base tumors has an established role. This report provides additional evidence of the value of radiosurgery as a primary or adjuvant management for meningiomas.

L. Dade LUNSFORD, M.D., F.A.C.S.
Lars Leksell Professor of Neurosurgery
Distinguished Professor
The University of Pittsburgh
Pittsburgh, Pennsylvania, U.S.A.

SPECIAL REPORT
IHE-RO: CURRENT STATUS AND PROBLEM
日放腫会誌 J Jpn Soc Ther Radiol Oncol 21: 49-53, 2009

臨床医およびJASTROデータベース委員会の立場から

寺原 敦朗[*1], 沼崎 穂高[*2]

CURRENT STATUS AND PROBLEMS OF IHE-RO FROM THE POINT OF VIEW OF A CLINICIAN AND JASTRO DATABASE COMMITTEE

Atsuro TERAHARA[*1], Hodaka NUMASAKI[*2]

Abstract: There are many issues regarding the input, management, and operation of information related to radiotherapy. In our department of radiation oncology, we reconstructed an old department database (DB) system, which had been utilized for years. The reconstructed DB was intended to contain sufficient information for JASTRO structural surveys and other data requests by adding data items included in the ROGAD (Radiation Oncology Greater Area Database) and omitting tables and items that were not appropriate for the current situation. However, we could not extract sufficient data for JASTRO structural surveys because of the lack of data and incorrect input methods. The new RIS (radiology information system) installed in our department requires that physicians enter the same information as in the department DB. Information sharing between systems in our hospital does not function well, and the workload of medical staff in daily clinical practice is increasing. It is difficult for us to maintain high levels of motivation for data entry in this situation. It is necessary to establish an information system, the Japanese National Cancer Database (JNCDB), that can collect nationwide data for cancer treatment and build cooperation among cancer registration systems and cancer database systems through the activities of the IHE-RO and JASTRO database committee.

Key words: IHE-RO, JASTRO Database Committee, National Cancer Database, Cancer registration

はじめに

放射線治療は，ハード，ソフト両面で目覚ましい進歩を遂げており，医療の中でもIT(information technology)化が最も進んでいる分野の1つと思われる．しかしながら，放射線治療に関する膨大な情報をどのように入力，管理，運用し，さらに有効活用していくかについては，まだまだ問題が多いように思われる．IHE-ROの活動は，それらの問題点を解決していくために重要なものであると考えられるが，臨床現場におけるその認知度はまだまだ低い状況であり，今後の発展が望まれる．本稿では，一臨床医の立場から，筆者の所属している東京大学医学部附属病院(東大病院)放射線治療部門の現状について報告するとともに，JASTROデータベース委員会の立場から，放射線治療部門の情報管理について考察したい．

東大病院の現状

1. 放射線治療部門データベース

東京大学においては，以前から放射線治療部門データベース(部門DB)が構築運用されていた．当初はMELCOMベースのデータベースであり，新たに治療開始された患者データを入力するのみならず，診断情報および病理組織診断情報については，過去に遡って入力する作業も行っていた．1991年に当時PC(Apple Macintosh)用の唯一のリレーショナルデータベースであった4th Dimension(4D)を用いたデータベースシステムに移行した．それを機に，本格的なデータの入力が開始された．また，その後には，このデータベースシステムと連結した電子カルテシステムを独自に開発し，病棟カルテとして運用されていた[1]．

しかしながら，2007年7月の時点では，データベースシステム開発者や管理者の異動，またソフトウェアがバージョンアップされておらず，対応するハードも老朽化してきていたことなどにより，実質上システムの管理が困難な状態となっていた．そこで，この部門DBの再構築を行うこととし，2007年8月末にFilemakerベースのDBに移行した．4D上では，多数のテーブルとそれらの間のリレーションからなる複雑な階層構造のデータベースシステムであったが，新システムへの移行にあたっては，今後も必要とされると思われるテーブルのみを移行することとした．さらに，現状に合わなくなった項目を割愛したり，JASTROデータベース委員会で作成されているROGAD(Radiation Oncology Greater Area Database)[2]に含まれる項目を加えて，JASTROの構造調査への対応や，将来の全国規模のデータ収集への対応も可能となることを目指した．その結果，日常診療において入力する項目は増加することとなった．

[*1]東京大学医学部附属病院放射線科(〒113-8655 東京都文京区本郷7-3-1) (Department of Radiology, University of Tokyo Hospital) (7-3-1, Hongo, Bunkyo-ku, Tokyo 113-8655, JAPAN), [*2]大阪大学大学院医学系研究科医用物理工学講座 (Department of Medical Physics and Engineering, Osaka University Graduate School of Medicine)

2007年のJASTRO構造調査に際しては，この部門DBからデータを抽出することによっての対応を試みた．しかし，実際には，治療情報が入力されていないモダリティーがあったり，データの入力もれや入力方法の誤りなどのために，部門DBに入力されていたデータからだけでは正確なデータを抽出することはできず，データの追加入力や修正などの作業が必要であった．現在は，情報の正確性を少しでも向上させるために，各担当者が入力したデータを，カルテを参照しつつ，管理者がチェックしている．

2. 放射線治療部門RIS

当院では，放射線治療に関するRIS(radiology information system)が2008年 4 月に更新され，放射線治療のオーダーとして，照射開始前に担当医師がデータを入力することが必須となった．HIS(hospital information system)と同じベンダーであるため，HISとの連携は構築されているが，上記の部門DBとの連携がないため，同じような情報をこちらにも入力することが必要となっており，情報入力の負担が増加している．当初は，このRISにデータ入力をすることで，部門DBの一部として活用することも検討されたが，入力項目のカスタマイズに対応できないとのベンダーからの回答があり，断念した．結局，最低限の必須項目のみが入力されている状態であり，DBとしての使用を想定していないこともあって，データの信頼性も低くなっている．

3. 院内がん登録

東大病院も2008年 2 月にがん診療連携拠点病院に指定され，院内がん登録が本格的に開始された．以前から登録のシステムは東大独自のものが構築されており，その入力が義務付けられてはいたものの，実際にはあまり入力されていなかった．現在は医師の負担増加を避けることを目的として，院内がん登録室が設置され，入力専門の要員が確保されている．しかし，ここでも，HISとの連携はしているものの，各診療科の部門DBとの連携がないため，病理報告書や登録病名からがん患者を抽出し，カルテの記載を参照しながら，同様の情報を院内で再入力している状況となっている．

JASTROデータベース委員会の活動

1. 診療科DBの提供

放射線治療部門標準DBとして，以前から開発されてきていたROGAD[2]を公表し，JASTROホームページ(http://www.jastro.jp/report/topic/070423.html)からdownload可能としている．さらに，現在，乳癌，食道癌，子宮頸癌，肺癌，前立腺癌の 5 疾患について，より詳細な各論DBを作成しており，これらについても近い将来に，JASTROホームページからdownload可能とするよう調整中である．個人情報部分は「院内がん登録」と一致させており，連携可能となるように考えている．また，すべてのDBソフトをオープンソース化し，各施設で改変可能な形式としており，施設の診療科DBとして汎用性が高く，利用価値の高いものになるものと考えている．

2. 構造調査データの公表

全国放射線治療施設の構造調査を定期的に行い，そのデータを公表してきた．このデータは，わが国における放射線治療のおかれている現状を正確に把握し，国や地方自治体における施策の提言，個々の医療機関における構造の改善に役立てることを最終目標としている．2005年定期構造調査の結果は，すでにJASTROホームページに公表されており[3]，JASTRO誌等にその解説も併せて報告されている[4-6]．

その解析の結果によると，放射線治療担当医の実質的マンパワーFTE(full time equivalent)当たりの年間実患者数は247人であった．がん診療連携拠点病院とその他の放射線治療施設に分けて，その分布をFig. 1 に示す[7]．放射線腫瘍医の患者負荷は前者で252人，後者では240人となっており，多少の差はあるものの，いずれも日米ブルーブックの基準である年間200人を超えていた[8, 9]．また，がん診療連携拠点病院の24%およびその他の施設の11%では，年間300名の改善警告値を超えた治療が行われていた．以前から指摘されてきた通り，放射線腫瘍医が不足しており，その負担が過重なものとなっていることが明らかである．

考　察

東大病院における放射線治療部門を含めた情報管理について報告をした．このように東大病院内だけでも，部門DB，放射線治療部門RIS，院内がん登録といった種々の情報系の間で，情報の共有がうまく行われていないために，同様の情報を二重，三重に入力することとなり，患者数の増加と相まって，現場の負担は増え続けている．DBへの情報入力そのものは，日々の患者の治療という点からは必須の業務ではなく，また，入力自体が治療成績の向上に直接結びつくものでもない．多忙な日常業務の中ではどうしても優先順位が低くなりがちであり，気が付くと，未入力やチェック待ちのデータが膨大に溜まってしまいがちである．このような状況でデータ入力が義務化されても，その意義を感じられなければ，実際の情報入力者である担当医のモチベーションは上がらず，情報の正確性が低下してしまい，その結果，データの信頼性が損なわれるために，情報入力の意義がますます低下してしまうという悪循環に陥りかねない．JASTRO構造調査以外にも，放射線治療に関するデータの提出を依頼されることが少なくないが，依頼される情報の内容はさまざまであり，部門DBやRISに登録されているデータのみで，それらすべてに対応することはできない．また，研究として治療成績の解析を行う際にも，部門DBの情報だけでは，対象となりうる症例のリストを抽出することができる程度で，詳細な解析を行うために